RESEARCH ARTICLE

Application of transfer learning in geoenvironmental evaluation of abandoned mines

Wenchao Wang*

The Fifth Prospecting Team of Shandong Coal Geology Bureau, Jinan, Shandong, China.

Received: February 27, 2024; **accepted:** April 12, 2024.

In the field of environmental science, the geoenvironmental problems caused by abandoned mines have been the focus of assessment and restoration efforts. To perform geoenvironmental evaluation of abandoned mines, the study utilized migration learning techniques to recognize remote sensing images of abandoned mines in the study area. The study integrated transfer learning with neural networks, enhanced the structure of convolutional neural networks by adding a similar feature layer, and used the long short-term memory structure for temporal feature transfer learning in order to improve the recognition accuracy of remote sensing images and, consequently, the accuracy of geoenvironmental evaluation. The results revealed that the accuracy rate of fused transfer learning and improved neural network model reached 93.15% and 93.19% in the identification of mine map points and mine slopes, respectively. This research focused on the application of transfer learning in the geological environment evaluation of abandoned mines, which could more accurately identify and evaluate the geological environment problems of abandoned mines, so as to provide a scientific basis for taking effective restoration measures.

Keywords: transfer learning; abandoned mines; geoenvironmental assessment; image recognition.

***Corresponding author:** Wenchao Wang, The Fifth Prospecting Team of Shandong Coal Geology Bureau, Jinan 250100, Shandong, China. Email: dizhishiyan215@163.com.

Introduction

Geoenvironmental assessment (GEA) of abandoned mine (AM) is a complex and important topic. Globally, many mines are abandoned after extraction and their environmental impacts may last for decades or even centuries, which can lead to serious environmental problems such as soil erosion, groundwater contamination, biodiversity decline, and other long-term negative impacts on surrounding communities and ecosystems [1]. Therefore, an accurate and comprehensive assessment of the geologic environment of AM for effective remediation and management is essential. However, GEA of AM is a challenging task that mainly involves the processing and parsing of a large amount of geological, geochemical, and environmental data [2]. While current assessment techniques can yield the intended outcomes in certain situations, handling and interpreting vast volumes of data frequently necessitates a substantial commitment of resources and knowledge. These methods may not be accurate or efficient enough when dealing with large-scale or complex mining environments [3, 4]. The introduction of remote sensing (RS) technology has provided a new solution to this problem. RS imagery can break through the limitations of human and material

resources and solve the dilemma in the field of geological evaluation of mines. Furthermore, the ability of RS technology to access challenging and complex areas contributes to a thorough exploration of the mine's general environment. However, the recognition of RS images also requires a lot of manpower and time. In the meantime, a huge number of mine RS datasets must be accumulated for the remote sensing image recognition (RSIR) procedure, but obtaining these datasets is challenging because of data confidentiality [5].

Environmental testing in mines is crucial in various fields, and it has garnered the attention of many researchers. Ziętek *et al*. discussed the challenges of measuring air quality in deep underground mines and proposed a low-cost system of gas sensors and microcontrollers that utilized smartphones as computing and visualization resources. The system enabled real-time monitoring and recording of data inside the mine, as well as air quality measurement in deep underground mines. The results demonstrated that this system could provide miners with real-time and effective information about gas hazards [6]. Xue *et al*. created a pulsed gas test system based on pulsed nitrogen fatigue cracking technology to increase the efficiency with which fossil fuels were used and lower the likelihood of coal mine safety incidents. The system proved its feasibility in practical application by improving the gas yield and gas extraction efficiency in low permeability coal seams [7]. A prototype inspection robot based on an autonomous ground vehicle platform was created by Szrek *et al*. to increase the efficiency and safety of belt conveyor maintenance in deep mines. The design employed infrared thermography for identifying and accurately locating potential hot spots and the results showed that this design significantly reduced the safety risks faced by personnel [8].

RSIR plays an important role in AM geoenvironmental detection. To cope with the challenge of analyzing massive marine RS data, Li *et al*. designed a marine RS image classification system using deep learning techniques, which reviewed two deep learning frameworks for realizing marine RS image classification. The effectiveness was tested in the mapping of multiple marine RS image types. The results indicated that the system had significant advantages in image information extraction compared with traditional physical or statistical based algorithms [9]. To save maintenance costs and improve the pace at which damaged crosswalks are located, Chen *et al*. created an autonomous crosswalk detection method based on RS images. To improve its robustness, the system suggested a road area guided crosswalk detection framework based on U-Net. Additionally, a hybrid classification technique was suggested, which combined the road region instruction for final crosswalk detection with the detection confidence. Road region guidance was useful for crosswalk detection and could enhance detection performance according to the experimental data [10]. A deep hashing convolutional neural network (CNN) was suggested by Song *et al*. as a solution to the problems with the RS image retrieval procedure. The results demonstrated that this method was able to achieve accurate retrieval and classification performance [11].

Although many efforts have been made in the research for mine environmental detection and RSIR, there are still relatively few studies on fusing transfer learning (TL) with neural networks (NNs) to detect AM geology for environmental evaluation. This study focused on the enhancement of the accuracy of RS image recognition for geological environment assessment in abandoned mining areas by utilizing TL technology and NNs to obtain more accurate environmental evaluation results. Similar feature layers were introduced to enhance the model's feature extraction ability. The long short-term memory (LSTM) networks were introduced to process and learn temporal features, improving the model's sensitivity to changes in RS images. The proposed model could be used to reveal the distribution characteristics of the geological environment and achieve precise zoning of the area, which would establish

a scientific foundation for the planning and development of future tourist resorts and offer practical recommendations for enhancing the ecological quality of the region.

Materials and methods

Identification of geologic environment of abandoned mine based on transfer learning

Each layer's architecture in conventional CNNs played a crucial role in the feature extraction procedure. An input layer, a pooling layer, a convolutional layer (CL), and a fully connected layer (FCL) were components of traditional CNNs [12]. In the CL that involved image feature extraction, each layer performed a convolutional operation to extract differential image features from the hierarchical structure. Low-level features were extracted by the forward layers, and as the layer's number, higher-level characteristics were extracted. However, the model runtime grew as the CNN layers got deeper. The non-recursive SimRank technique computed similarity values to extract the similar feature layer (SFL) and deeper features from an image in a shallower layer structure [13] (Figure 1). The extraction of SFLs was a key step in image-based data analysis, which was to transform one layer of image data into an k -layer image matrix, where the parameter k needed to be determined experimentally, and this process usually included node feature extraction, metrics of inter-node relationships, and construction of SFLs [14]. Each node had features such as attributes, degree, *etc*. and similarity between nodes could be calculated based on the relationship of edges. By constructing a similarity feature layer, nodes with high similarity were grouped together, which helped to extract higher level features. SimRank algorithm measured the similarity between nodes in the graph and calculated the association between nodes by iteration. The combination of node feature extraction, relationship metric, and SFL construction could effectively extract feature information from image data [15]. The calculation formula of SimRank algorithm to extract SFL was shown in equation (1).

$$S(a,b)=\frac{C}{|N(a)|\times|N(b)|\times\sum S(Ni(a),Nj(b))} \quad (1)$$

where $S(a,b)$ was the similarity between node a and node b . C was a constant that usually took values between 0 and 1. $|N(a)|$ and $|N(b)|$ were the neighbor nodes of node a and node b , respectively. $Ni(a)$ and $Nj(b)$ were the neighbor nodes of node a and node b . The NN model that was improved by adding SFL extraction was called SimCNN model. In a conventional CNN, the model was more likely to settle into local optimal solutions as the number of layers rose, which led to insufficient feature extraction. By using SFLs, SimCNN could more effectively capture the global properties of the image input, enhancing the model's stability and recognition accuracy. At the same time, SimCNN maximally maintained the invariance of data features during feature extraction, *i.e*. when dealing with complex image data, SimCNN was able to extract features more stably and reduced the impact of data noise and interference on model performance. The structure of SimCNN model based on source data feature migration was shown in Figure 2. The architecture of SimCNN was an extra SFL in the conventional CNN layer construction. This layer enhanced the model's performance and capacity for generalization by helping it to extract the deep characteristics of the picture input more effectively. This design allowed SimCNN to have higher efficiency and accuracy in processing complex image data. The primary dataset for performing TL was called the source dataset. For the source data of RS images, the feature TL involved various layer structures of the SimCNN model. Training the SimCNN model using the source dataset mainly involved forward propagation and backward propagation, the two main processes in NN training [16]. The input data was transported forward *via* the NN's multilayer structure until it reached the output

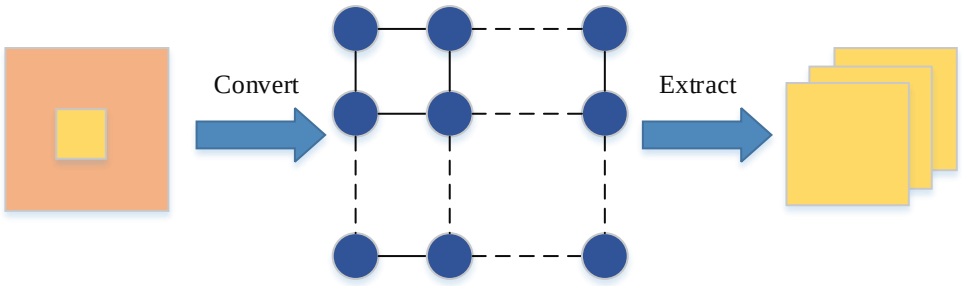

Figure 1. The extraction process of similar feature layers.

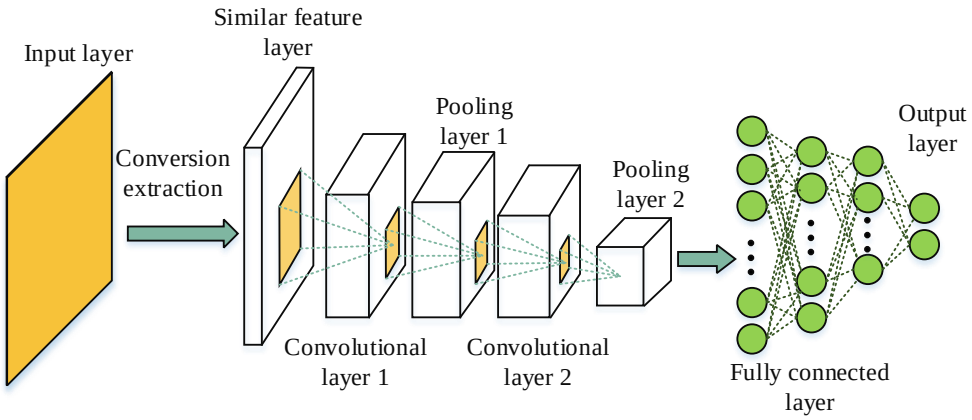

Figure 2. SimCNN model structure based on source data feature transfer.

layer during the forward propagation phase. The primary goal of this procedure was to compute each layer's output values and, in the end, obtained the network's forecast. On the other hand, a gradient descent technique was employed to update the model parameters throughout the backward propagation phase, where the gradient of the loss function with respect to the network parameters was computed. By following this procedure, it was guaranteed that the model would learn to minimize errors. Therefore, the loss was computed using forward propagation, and the model parameters were optimized and adjusted using backward propagation. Together, these two processes formed the core of NN training, ensuring that the model could effectively learn from the source dataset and migrate to new tasks. The calculation of the output prediction value was shown in Equation (2).

$$f_i^{N+1} = \sigma\left(\omega^N, ...\sigma\left(\omega^2\left(\sigma\left(\omega^1 a^1 + b^1\right) + b^2, ... + b^N\right)\right)\right) \quad (2)$$

where f_i^{N+1} was the output prediction value and N was the FCLs. ω was the weights. b was the bias value. σ was the $Sigmoid$ activation function. The loss function's mathematical expression (ME) was shown in Equation (3).

$$L\left(f_i^{N+1}, f_i\right) = \sum_{i=1}\left(\left(f_i\right)\log\left(f_i^{N+1}\right) + \left(1 - f_i\right)\log\left(1 - f_i^{N+1}\right)\right) \quad (3)$$

where L was the loss function and f_i was the true label. The ME for the correction weights of the gradient descent algorithm was shown in equation (4).

$$\omega^{N+1} = \omega^{N+1} - \varepsilon\frac{\partial N\left(f^{N+1}, f\right)}{\partial \omega^N} \quad (4)$$

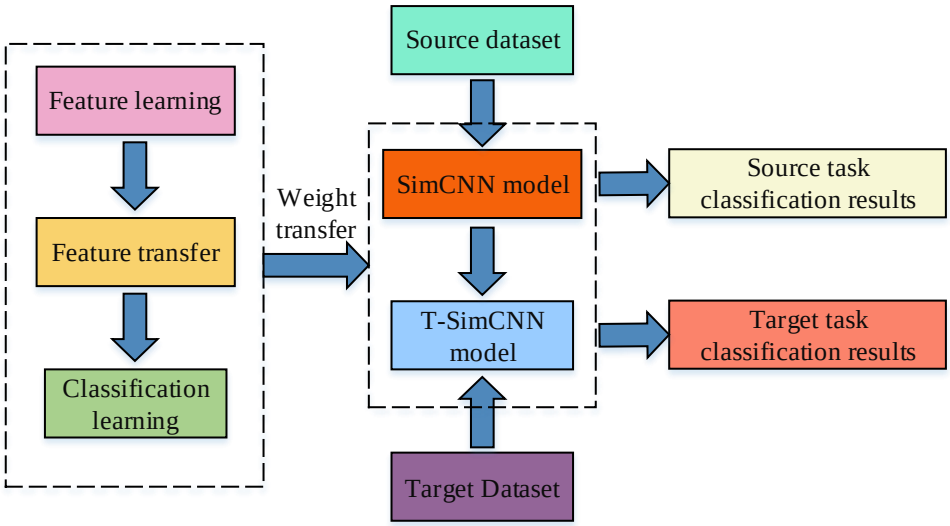

Figure 3. The process of source data features transfer learning.

where ω^{N+1} was the corrected weights and ε was the learning rate of TL. The ME for the modified bias value of the gradient descent algorithm was shown in equation (5).

$$b^{N+1} = b^{N+1} - \varepsilon \frac{\partial N\left(f^{N+1}, f\right)}{\partial b^{N}} \quad (5)$$

The process of updating the model parameter weights and biases as shown in equation (4) and (5) was to minimize the loss function. TL of source data features was achieved by applying the updated parameters to the new model. The process of TL of source data features was shown in Figure 3. After training on the source dataset, the SimCNN pre-trained model based on the source dataset could be obtained. The new model T-SimCNN after TL could be further obtained by weight migration according to the feature migration strategy of TL. TL involved applying the features that the model had learned to the target task once it had been trained on a sizable pre-training dataset. A specifically created TL technique transferred the parameters acquired from the source dataset to the target domain on the pre-trained CL, which effectively addressed the issue of the model's short source dataset size and challenging convergence, enhancing the model's accuracy and capacity for generalization of particular tasks.

SimCNN model-based temporal feature migration

The SimCNN model was used to perform temporal feature migration in order to properly account for the temporal aspects of RS images and further increase the recognition effect of the improved technique based on the combination of NN and TL. One particular type of recurrent NN that performed exceptionally well when handling time-series data was called LSTM [17]. The study used the LSTM-NN structure for time-series feature migration in order to let the SimCNN model absorb time-series data features while maintaining the features of the source dataset (Figure 4). When the time series data were processed into the internal structural units of the LSTM-NN, the temporal properties of the waveform time series data were recovered [18]. Subsequently, an FCL with 512 neurons was connected to transfer the output of the LSTM to the fully connected neurons. Two neurons for classification were connected to accomplish the task of classifying the time series data. LSTM performed well in processing time-series data and was able to capture and convey temporal features effectively. Conversely, SimCNN could

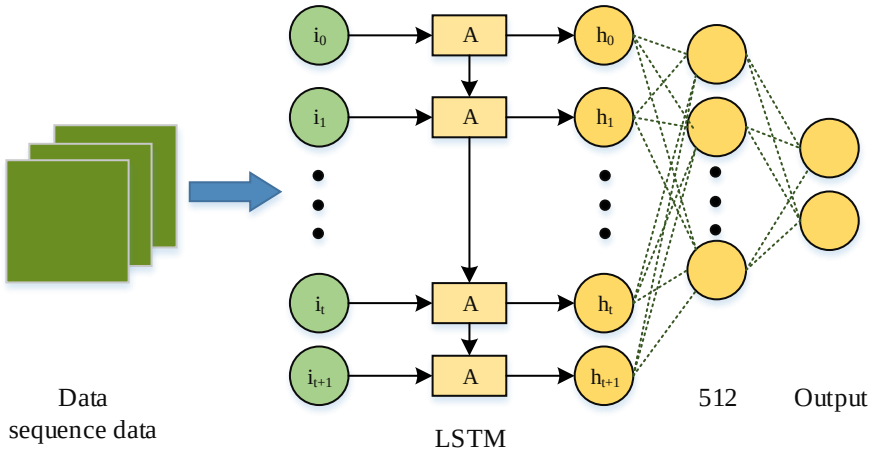

Figure 4. LSTM neural network structure based on temporal feature transfer.

extract significant features from the data and possessed a robust feature extraction capability. This combination enhanced the model's stability and identification accuracy while allowing it to handle RS image data with temporal aspects more effectively. The ME for the input gate of the LSTM network was shown in equation (6).

$$i_t = \sigma\left(\omega_i * \left(h_{t-1}, x_t\right) + b_i\right) \tag{6}$$

where i_t was the input gate. t was the moment. h_{t-1} was the hidden layer state of the previous moment. Equation (7) displayed the ME forgetting gate.

$$y_t = \sigma\left(\omega_y * \left(h_{t-1}, x_t\right) + b_y\right) \tag{7}$$

where y_t was the oblivious gate. The ME for the hidden layer was shown in Equation (8).

$$h_t = o_t * \tanh\left(C_t\right) \tag{8}$$

where o_t was the output gate. h_t was the hidden layer. C_t was the memory cell. $\tanh$ was the activation function. The ME of the output gate was shown in Equation (9).

$$o_t = \sigma\left(\omega_o * \left(h_{t-1}, x_t\right) + b_o\right) \tag{9}$$

The ME for the memory unit was shown in Equation (10).

$$C_t = y_t * C_{t-1} + i * C_t' \tag{10}$$

where C_t' was the updated memory unit. The ME for C_t' was shown in Equation (11).

$$C_t' = \tanh\left(\omega_C * \left(h_{t-1}, x_t\right) + b_C\right) \tag{11}$$

The optimization of the model was implemented through a backpropagation process, in which the error flew backwards layer by layer along the network, and the gradient generated by the trans-chaining law adjusted and optimized the forward propagation parameters of the model [19]. The process of optimizing the gradient *via* the chain rule was shown in Equation (12).

$$\frac{\partial L}{\partial \omega_y} = \sum_{t=1}^{T} \frac{\partial L}{\partial C^t} \frac{\partial C^t}{\partial y^t} \frac{\partial y^t}{\partial \omega_y} = \frac{\partial L}{\partial C^t} \tag{12}$$

The LSTM-NN model gradually adjusted its parameters to achieve the continuous improvement of the classification accuracy while minimizing the classification error [20]. This mechanism not only optimized the feature extraction capability of LSTM, but also refined its parameter training process. This model structure

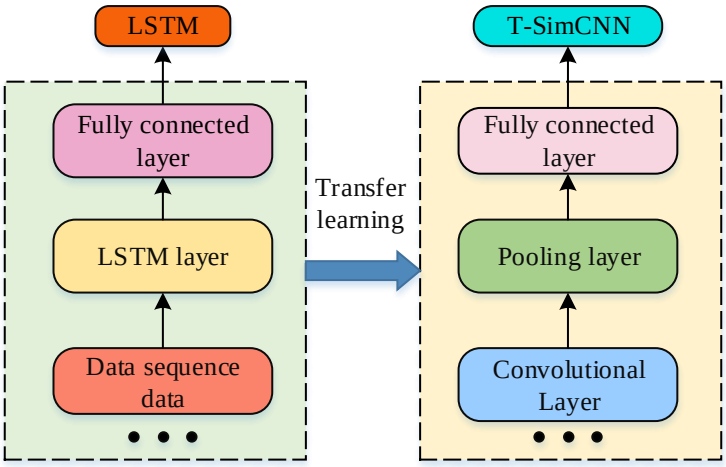

Figure 5. The process of temporal feature transfer learning.

was particularly suitable for dealing with the long-term dependence of time series data, effectively avoiding the problem of gradient vanishing, which was common in sequence processing, and ensuring that the long-range temporal information was fully utilized. The process of time series feature TL was shown in Figure 5. The pre-trained LSTM-NN model using TL migrated the features of these parameters into the second FCL of the new model T-SimCNN after receiving the weights and bias values of the FCL. This step implemented the migration from the source time series dataset features to the T-SimCNN model. In this way, it was possible to introduce the advantages of LSTM-NNs in processing time series data into the T-SimCNN model. This not only increased the model's capacity to extract temporal features, but it also made the model more stable and accurate at recognizing features while processing RS image data that had temporal aspects. After feature migration, the output of the FCL was carried out using the $soft\max$ function, and the weight partial derivatives of the $N+1$ th FCL were shown in Equation (13).

$$\frac{\partial N\left(f_i^{N+1}, f_i\right)}{\partial \omega_{i,j}^{N+1}} = \sum_{i=1}\left(\frac{-f_i}{f_i^{N+1}} + \frac{1-f}{1-f_i^{N+1}}\right)\sigma\left(\sum_{i=1}^{i}\omega_{i,j}a^N + b^{N+1}\right) \quad (13)$$

The partial derivatives of the bias values of the FCLs of layer N were shown in Equation (14).

$$\frac{\partial N\left(f_i^{N+1}, f_i\right)}{\partial b_i^N} = \sum_{i=1}\frac{v_i^{N+1} - f_i}{v_i^{N+1}\left(1-v_i^{N+1}\right)} \quad (14)$$

where v_i was the element of vector v in the previous layer. The output value of the FCL was shown in Equation (15).

$$Soft\max\left(v_i\right) = \frac{\exp\left(v_i\right)}{\sum_j \exp\left(v_j\right)} \quad (15)$$

where v_j was the element of vector v in the next layer. The $soft\max$ function was able to normalize the data passed by the input from the previous layer to the next layer and finally output a probability value between 0 and 1. Mines had the phenomena of land resources being suppressed and topography and landscape being destroyed due to mining problems, so the study utilized the *Code of Investigation and Evaluation of Mine Geological Environment* to evaluate the mine geological environment in zones based on the results of AMGEI combined with the uniqueness of AM. The study separated the AM into two areas for evaluation including mine slopes and mine map points based on the results of fieldwork and RS image geoenvironmental identification. The evaluation level was categorized into three levels including light, ordinary, and serious according to the degree of

Table 1. Specific experimental environment configuration.

Hardware		Software environment	
Experimental environment	**Configuration**	**Experimental environment**	**Configuration**
OS system	Windows10	Programming Language Environment	Python 3.7
CPU	Intel(R) Core(TM) i5-4460	Deep learning network model training platform	TensorFlow 1.14.0
GPU	NVIDIA Titan Black GPU	Programming software	PyCharm 2019.1.1
Memory	64GB	Data visualization library	Matplotlib 3.0.3
Hard disk	512GB	Data processing library	Numpy 1.16.2

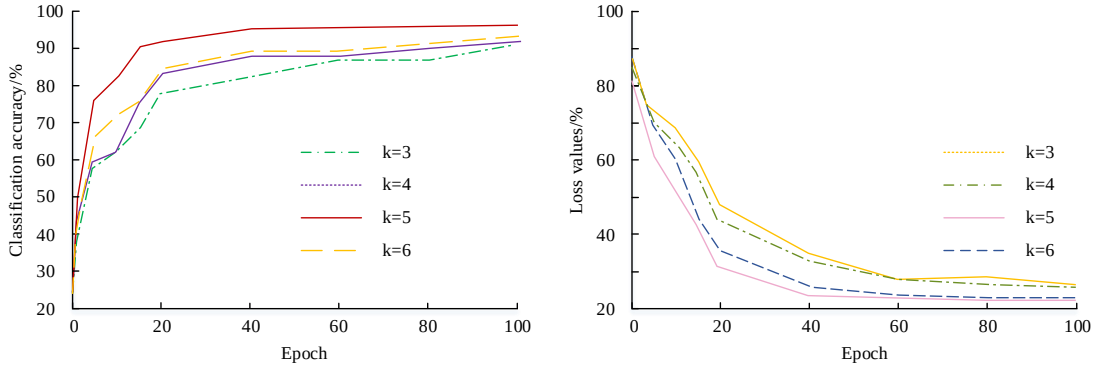

(a) Classification accuracy of different k values (b) Loss values for different k values

Figure 6. The variation curves of classification accuracy and loss value for different values.

damage to the topographic landscape. When the degree of damage exceeded 40%, it was recognized as serious. When it was less than 20%, it was recognized as light. The rest of the degree of damage was recognized as ordinary. The combination of NN and TL for AMGEI and evaluation of RS images was used to obtain more accurate environmental evaluation results and provide a reliable basis for geoenvironmental analysis for subsequent restoration and engineering development of the AM area.

Experimental environment

The experimental environment of this study was constructed based on both hardware and software. The datasets used included publicly available RS datasets including WHU-RS19 and SIRI-WHU datasets (Wuhan University, Wuhan, Hubei, China), UC Merced Land-Use dataset (University of California Merced, Merced, CA, USA), and Bijie landslide dataset (Bijie, Guizhou, China). The study split these datasets into training and testing sets in a 6:4 ratio. The model settings used in this study were that the learning rate was set to 0.0005, the number of training times was set to 100, the batch sample sizes were set to 200 and 32, and the default optimization algorithm was the Adam optimization algorithm. The value was set to 0.0001 for L2 regularization, and the Dropout setting was set to 0.5. The precise configuration information for the experimental environment was listed in Table 1.

Results and discussion

Performance validation of transfer learning-based geologic environment identification in abandoned mine

To determine the optimal value of the parameter k, the study conducted 100 training cycle iterations and set the k value in the range of 3 to 6. The variation curves of classification accuracy and loss value for various k values during the training procedure were shown in Figure 6. When the training cycle reached 40 times, the training

accuracies of different k values all showed a convergence trend (Figure 6a). The highest accuracy of 95.57% was achieved at k value of 5, which was an improvement of 4.53%, 3.70%, and 2.08% compared to the accuracies at k values of 3, 4, and 6, respectively. When the k value was 5, the loss function had the lowest value of 12.41%. Meanwhile, the loss function curve converged faster and was more stable compared to the curves at other k values (Figure 6b). Based on the above results, the model functioned best when the k number was 5.

The study compared the SimCNN model with the conventional CNN and LSTM models after setting parameter B to 5, which allowed for an evaluation of the model's performance. The study investigated the execution times of these three models using the UC Merced Land-Use, Bijie landslide, SIRI-WHU, and WHU-RS19 datasets (Figure 7). The running time of the SimCNN model was marginally longer than that of the LSTM model due to the LSTM model having fewer layers, but it was still significantly faster than the CNN model. Specifically, the running time of SimCNN model in the four datasets was 10.65, 11.58, 9.48, and 10.97 ms, which was reduced by 50.55%, 50.86%, 54.79%, and 51.54%, respectively, compared with the CNN model. Therefore, the optimization made by the SimCNN model on the basis of the traditional CNN model effectively improved the running efficiency.

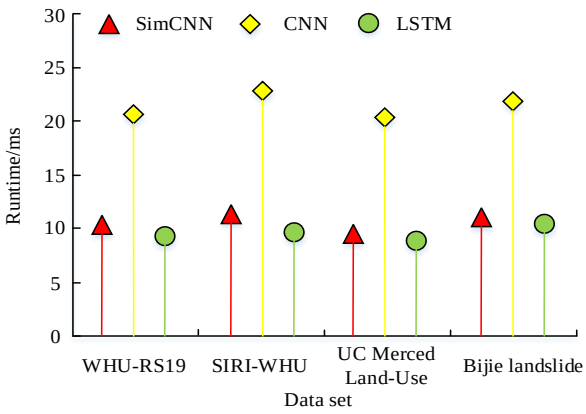

Figure 7. Comparison of runtime of models in different datasets.

The comparison of the SimCNN model's performance in terms of classification accuracy and loss value with the classic CNN model and LSTM model demonstrated that the classification accuracy of the SimCNN model was significantly higher than that of the other two models, reaching 95.04%. Compared to the 90.67% accuracy of the CNN model and the 88.49% accuracy of the LSTM model, the SimCNN model improved the accuracy by 4.37% and 6.55%, respectively (Figure 8a). Furthermore, the SimCNN model's loss value was 7.91%, which was 3.73% and 11.03% less than that of the CNN (11.64%) and LSTM model (18.94%), respectively. Therefore, the SimCNN model was better than other models in terms of performance.

Performance validation of transfer learning model for abandoned mines geological environment

The study obtained the T-SimCNN model with temporal and source features by TL. Model training was done first to validate the model's performance. The T-SimCNN model training outcomes showed that the model's classification accuracy stabilized at 95% when 40 iterations or more were performed (Figure 9). In the meantime, the model's loss function value steadily got closer to 0 as the number of iterations rose. The results demonstrated the great degree of stability and quick convergence of the T-SimCNN model, demonstrating its superior fitting capability. Thus, TL had resulted in the T-SimCNN model having a high degree of fitting. The total loss and classification loss of the T-SimCNN model in the four datasets were compared and validated to confirm the efficacy of TL. The T-SimCNN model displayed the smallest total loss in the SIRI-WHU dataset, down to 10.46% (Figure 10a). Compared to the total loss values in the UC Merced Land-Use dataset, the WHU-RS19 dataset, and the Bijie landslide dataset, the total loss of the T-SimCNN model was reduced by 12.58%, 7.18%, and 6.11%, respectively. The T-SimCNN model also showed the smallest classification loss of 7.98% in the SIRI-WHU dataset (Figure 10b). Compared with the classification loss values in the UC Merced

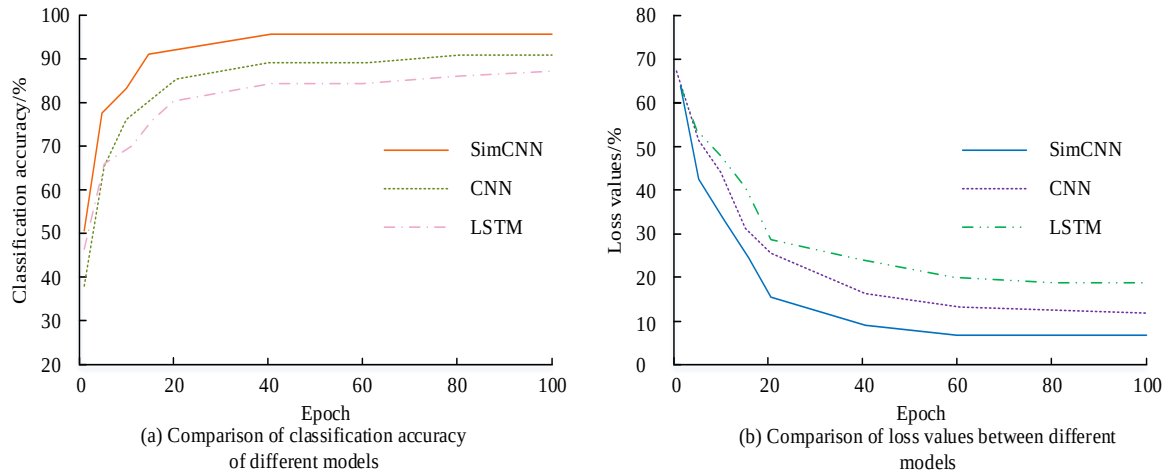

Figure 8. Comparison of classification accuracy and loss values of different models.

Table 2. Evaluation results of geological environment in abandoned mines.

Environment	Recognition	SimCNN	T-SimCNN	Field investigation	Artificial visual inspection
Mining area map spot	Number of images	73.00	73.00	73	73.00
	Identify the correct quantity	62.00	68.00	73	72.00
	Accuracy/%	84.93	93.15	100	98.63
Mine slope	Number of images	88.00	88.00	88	88.00
	Identify the correct quantity	75.00	82.00	88	86.00
	Accuracy/%	85.22	93.19	100	97.72

Land-Use dataset, the WHU-RS19 dataset, and the Bijie landslide dataset, the classification loss of the T-SimCNN model was reduced by 14.11%, 9.91%, and 8.52%, respectively. Therefore, in general, the T-SimCNN model with TL showed excellent performance.

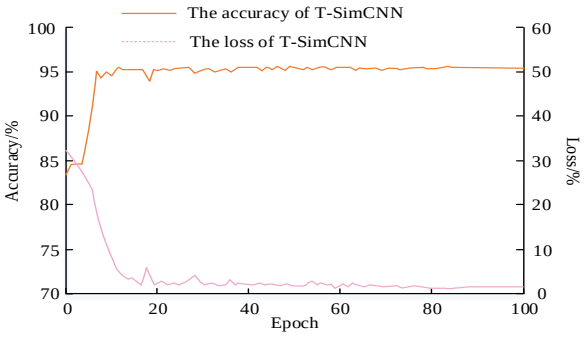

Figure 9. Training results of T-SimCNN model.

To validate the performance of the TLT-SimCNN model in real-world applications, the study conducted fieldwork in 88 AMs. The AMs were also captured in far and near views, and the resulting images were processed into a validation set. Among the mine map points and mine slope areas in these 88 AMs, there were 21 and 39 locations with severe GEA ratings, 28 and 35 locations with normal GEA ratings, and 18 and 15 locations with lighter GEA ratings, respectively. The study compared and analyzed the evaluation results of T-SimCNN model and manual survey for these three GEA grade locations, and the evaluation results of AM geological environment were shown in Table 2. The accuracies of SimCNN and T-SimCNN were 84.93% and 93.15% for the recognition and evaluation of the map points in the mining area, while the accuracies of field survey and manual visual inspection were 100% and 98.63%, respectively. For the recognition and evaluation of mine slopes, the accuracies of

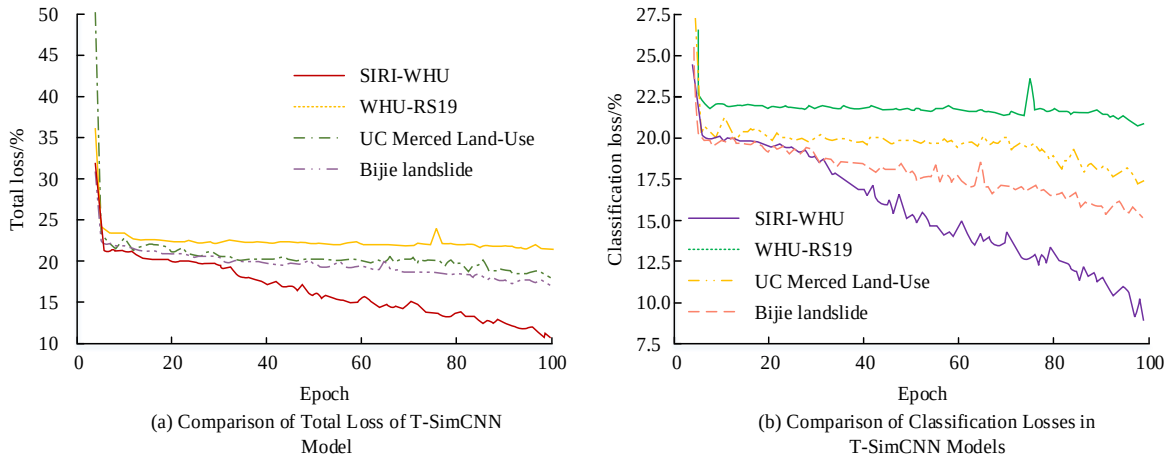

Figure 10. Comparison of total loss and classification loss of T-SimCNN model.

SimCNN and T-SimCNN were 85.22% and 93.19%, respectively, while the accuracies of field survey and manual visual inspection were 100% and 97.72%, respectively. The T-SimCNN model's evaluation accuracy was marginally lower than that of the field survey and manual visual inspection while being greater than the SimCNN model in both scenarios. Although T-SimCNN could not completely replace the field survey and manual visual inspection, the T-SimCNN model still had high accuracy and could be used as a powerful complement to the field survey and manual visual inspection.

Conclusion

Assessing the geological environment in AMs is crucial for environmental protection. It has a profound impact on monitoring environmental risks and protecting the ecological environment. However, conventional environmental assessment methods often require extensive on-site investigation and visual inspection, which is labor-intensive and inefficient. To tackle this issue, the Transfer Learning SimCNN model had been applied to identify and assess the geological environment of legacy mines. The study revealed that the SimCNN model not only improved the classification accuracy, but also reduced the running time compared to CNN models. After applying transfer learning, the T-SimCNN model achieved the lowest total loss in the SIRI-WHU dataset and demonstrated excellent performance. In practical applications, it had proven highly accurate in identifying map points and mine slopes in mining areas. Comprehensive analysis indicated that both the SimCNN and T-SimCNN models exhibited high accuracy and efficiency in identifying and evaluating the geological environment of legacy mines. While transfer learning could not fully replace field investigations and visual inspections, it had significant value in evaluating the geological environment of Ams, which offered new approaches and techniques for addressing the geological and environmental issues caused by AMs.

References

1. Niu S, Liu Y, Wang J, Song, H. 2020. A decade survey of transfer learning (2010-2020). IEEE Transactions on Artificial Intelligence. 1(2):151-166.
2. Salom AT, Kivinen S. 2020. Closed and abandoned mines in Namibia: A critical review of environmental impacts and constraints to rehabilitation. South African Geographical Journal. 102(3):389-405.
3. Tammina S. 2019. Transfer learning using vgg-16 with deep convolutional neural network for classifying images. International Journal of Scientific and Research Publications (IJSRP). 9(10):143-150.

4. Raffel C, Shazeer N, Roberts A, Lee K, Narang S, Matena M, *et al*. 2020. Exploring the limits of transfer learning with a unified text-to-text transformer. J Mach Learn Res. 21(1):5485-5551.
5. Hebbi C, Mamatha H. 2023. Comprehensive dataset building and recognition of isolated handwritten Kannada characters using machine learning models. Artificial Intelligence and Applications. 1(3):179-190.
6. Ziętek B, Banasiewicz A, Zimroz R, Szrek J, Gola S. 2020. A portable environmental data-monitoring system for air hazard evaluation in deep underground mines. Energies. 13(23):6331-6335.
7. Xue Y, Liu J, Ranjith PG, Gao FH, Wang J. 2022. Changes in microstructure and mechanical properties of low-permeability coal induced by pulsating nitrogen fatigue fracturing tests. Rock Mech Rock Eng. 55(12):7469-7488.
8. Szrek J, Wodecki J, Błażej R, Zimroz R. 2020. An inspection robot for belt conveyor maintenance in underground mine-Infrared thermography for overheated idlers detection. Applied Sciences. 10(14):4984-4991.
9. Li X, Liu B, Zheng G, Ren Y, Zhang S, Liu Y, *et al*. 2020. Deep-learning-based information mining from ocean remote-sensing imagery. Natl Sci Rev. 7(10):1584-1605.
10. Chen Z, Luo R, Li J, Du J, Wang C. 2021. U-Net based road area guidance for crosswalks detection from remote sensing images. Can J Remote Sens. 47(1):83-99.
11. Song W, Li S, Benediktsson JA. 2020. Deep hashing learning for visual and semantic retrieval of remote sensing images. IEEE Trans Geosci Remote Sens. 59(11):9661-9672.
12. Liu R, Xu Y, Rui HC, El-Wardany RM, Dong Y. 2021. Migration and speciation transformation mechanisms of mercury in undercurrent zones of the Tongguan gold mining area, Shaanxi Loess Plateau and impact on the environment. China Geology. 4(2):311-328.
13. Peng D, Bruzzone L, Zhang Y, Guan H, Ding H, Huang X. 2020. SemiCDNet: A semisupervised convolutional neural network for change detection in high resolution remote-sensing images. IEEE Trans Geosci Remote Sens. 59(7):5891-5906.
14. Shahmoradi J, Talebi E, Roghanchi P, Hassanalian M. 2020. A comprehensive review of applications of drone technology in the mining industry. Drones. 4(3):34-40.
15. Chen H, Wu C, Du B, Zhang L, Wang L. 2019. Change detection in multisource VHR images *via* deep siamese convolutional multiple-layers recurrent neural network. IEEE Trans Geosci Remote Sens. 58(4):2848-2864.
16. Li X, Zhou T, Li J, Zhou Y, Zhang Z. 2021. Group-wise semantic mining for weakly supervised semantic segmentation. Proceedings of the AAAI Conference on Artificial Intelligence. 35(3):1984-1992.
17. Chouhan V, Singh SK, Khamparia A, Gupta D, Tiwari P, Moreira C, *et al*. 2020. A novel transfer learning based approach for pneumonia detection in chest X-ray images. Applied Sciences. 10(2):559-605.
18. Das NN, Kumar N, Kaur M, Kumar V, Singh D. 2022. Automated deep transfer learning-based approach for detection of COVID-19 infection in chest X-rays. Irbm. 43(2):114-119.
19. Chen Y, Qin X, Wang J, Yu C, Gao W. 2020. Fedhealth: A federated transfer learning framework for wearable healthcare. IEEE Intell Syst. 35(4):83-93.
20. Pathak Y, Shukla PK, Tiwari A, Stalin S, Singh S. 2022. Deep transfer learning based classification model for COVID-19 disease. Irbm. 43(2):87-92.